ORIGINAL PAPER



An experimentally calibrated thermobarometric solubility model for titanium in coesite (TitaniC)

Zach R. Osborne¹ • Jay B. Thomas¹ • William O. Nachlas¹ • Suzanne L. Baldwin¹ • Megan E. Holycross² • Frank S. Spear³ • E. Bruce Watson³

Received: 7 February 2019 / Accepted: 17 April 2019 / Published online: 25 April 2019 © Springer-Verlag GmbH Germany, part of Springer Nature 2019

Abstract

Experiments were conducted to quantify the temperature and pressure effects on the solubility of titanium in coesite. Powdered amorphous silica, titania (anatase), zirconia, and water were added to silver capsules and run in the coesite stability field (at 32, 35, and 40 kbar) from 700 to 1050 °C using a piston–cylinder apparatus. Crystallization of coesite, rutile, and zircon from silica-, titania-, and zircon-saturated aqueous fluids was confirmed by Raman spectroscopy. Cathodoluminescence images and electron microprobe measurements showed that coesite crystals are relatively homogenous. The Ti concentrations of coesite crystals are significantly higher than concentrations predicted using the Ti-in-quartz calibration (Wark and Watson in Contrib Mineral Petrol 152:743–754, 2006. https://doi.org/10.1007/s00410-006-0132-1; Thomas et al. in Contrib Mineral Petrol 160:743–759, 2010. https://doi.org/10.1007/s00410-010-0505-3). Titanium K-edge X-ray absorption near edge structure (XANES) measurements demonstrate that Ti⁴⁺ substitutes for Si⁴⁺ on fourfold tetrahedral sites in coesite at all conditions studied. A model was calibrated to describe the effects of pressure and temperature on the solubility of titanium in coesite by using a least-squares method to fit Ti concentrations in coesite to the simple expression:

$$RT \ln X_{\text{TiO}_2}^{\text{coesite}} = -55.068 + 0.00195 \times T \text{ (K)} - 1.234 \times P \text{ (kbar)} + RT \ln a_{\text{TiO}_2}^{\text{rutile}}$$

where R is the gas constant 8.3145×10^{-3} kJ/K, P is pressure in kbar, T is temperature in kelvin, $X_{\text{TiO}_2}^{\text{coesite}}$ is the mole fraction of TiO_2 in coesite, and $a_{\text{TiO}_2}^{\text{rutile}}$ is the activity of TiO_2 in the system referenced to rutile. Ti-in-coesite solubility can be used as a thermobarometer for natural samples when used in combination with another indicator of temperature or pressure, such as another thermobarometer in a cogenetic mineral (e.g. rutile) or other phase equilibria (e.g. graphite = diamond). Applications of the Ti-in-coesite thermobarometer to samples from the western Alps and Papua New Guinea are presented.

Keywords Coesite \cdot Ti in coesite \cdot Thermobarometer \cdot Thermobarometry \cdot Rutile \cdot Zr in rutile

Communicated by Mark Ghiorso.

- Zach R. Osborne
 zrosborn@syr.edu
- ¹ 204 Heroy Geology Laboratory, Department of Earth Sciences, Syracuse University, Syracuse, NY 13244, USA
- Department of Mineral Sciences, National Museum of Natural History, Smithsonian Institution, Washington, DC 20560, USA
- Department of Earth and Environmental Sciences, Rensselaer Polytechnic Institute, Troy, NY 12180, USA

Introduction

Loring Coes Jr. first reported on his synthesis of a previously unknown crystalline silica in the early 1950s, additionally noting that it was possible the natural existence of this higher-pressure polymorph of quartz had been overlooked (Coes 1953). Subsequent discovery of this dense silica in nature (Chao et al. 1960) at Barringer Crater was the necessary catalyst for the acceptance of coesite as a verified mineral (Hazen 1999). The potential usage of coesite as an index mineral for metamorphic petrology and tectonics was not realized for several more decades. Discovery of coesite in the western Alps of Italy (Chopin 1984) and in the



Western Gneiss Region of Norway (Smith 1984) presented direct evidence that continental crust could be transported to depths greater than 100 km and then exhumed as the result of tectonic processes; these processes are included under the umbrella of ultrahigh-pressure (UHP) metamorphism (i.e. pressures greater than ~25 kbar). Until our study, coesite could be used only to indicate metamorphism at ultrahigh pressures; it has not been possible to quantify an exact pressure and temperature of natural coesite formation.

Previous studies have experimentally quantified the pressure-temperature dependencies of Ti solubility in quartz (Wark and Watson 2006; Ostapenko et al. 2007; Thomas et al. 2010, 2015). Several studies involved mineral synthesis experiments where Ti was incorporated into quartz during co-crystallization of quartz and rutile (TiO₂). The synthesis experiments of Thomas et al. (2010) established and later confirmed (Thomas et al. 2015) that Ti-in-quartz solubility is strongly dependent upon temperature and pressure. The Ti-in-quartz solubility data were fit to a simple thermodynamic expression or 'calibration' for subsequent application as a thermobarometer to natural samples. However, the Thomas et al. (2010) Ti-in-quartz thermobarometer cannot be accurately applied to silica minerals formed at pressures outside the quartz stability field. We conducted experiments in the coesite stability field over temperatures from 700 to 1050 °C and pressures of 32, 35, and 40 kbar. The concentration of Ti incorporated into coesite was controlled by cocrystallizing coesite, rutile, and zircon from hydrothermal fluids in the SiO₂-TiO₂-ZrO₂ system. Raman spectroscopy was used to identify synthesized minerals. Titanium K-edge X-ray absorption near-edge structure measurements confirm that Ti⁴⁺ substituted for Si⁴⁺ on fourfold tetrahedral sites in the coesite lattice at all pressures. We present a titaniumin-coesite solubility model that can be used as a thermobarometer for natural samples when used in combination with another indicator of temperature or pressure, such as another thermobarometer in a cogenetic mineral (e.g. rutile) or other phase equilibria (e.g. graphite = diamond).

Methods

Experiments

Experiments were conducted using an end-loaded piston–cylinder apparatus designed after Boyd and England (1960a). A half-inch diameter piston–cylinder assembly with crushable materials (MgO–Pyrex–NaCl: Watson et al. 2002; Thomas et al. 2010, 2015) was used in all experiments (Fig. 1). Silver capsules with ~1 mm thick walls (~20 mm³ in volume) contained the powdered Alfa Aesar starting materials of SiO₂ (~10 mg, amorphous), TiO₂ (~3 mg, anatase), and ZrO₂ (~5 mg), and H₂O (deionized). The amounts of

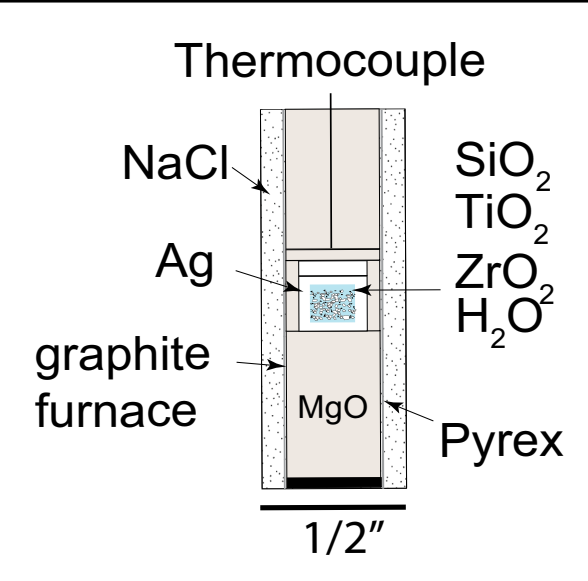


Fig. 1 Piston-cylinder assembly used in all experiments

powdered starting materials were relatively consistent for each experiment; the amount of water added to the capsule varied depending on the intended P-T conditions, with less added at higher pressures and temperatures. Experimental capsules were sealed in piston-cylinder vessels during pressurization at room temperature. Hydraulic oil pressures were measured with Enerpac Bourdon-tube gauges with 18 cmdiameter dials. Experiments were run at pressures of 30, 32, 35 and 40 kbar, and temperatures from 700 to 1050 °C (Fig. 2) spanning all potential coesite-quartz phase boundaries. Temperature was controlled to ± 1 °C using type-D thermocouples (W₉₇Re₃–W₇₅Re₂₅) and Eurotherm Nanodac PID controllers; thermocouple accuracy reported from the vendor (Concept Alloys) is ±0.5 °C. Small pressure adjustments were typically needed during heating to the final run temperature, after which pressure usually remained relatively consistent for experimental duration. Small increases were made to maintain pressure if necessary; oil pressure was usually adjusted if it dropped ~ 200 psi beneath the target pressure, which is the smallest graduation on our pressure gauges (200 psi oil pressure equals 0.5 kbar experimental pressure). No 'friction corrections' were applied to the calculated experimental pressures because reported pressures are interpreted as accurate to within approximately \pm 120 bars (Spear et al. 2014; Thomas and Spear 2018). Six tungsten carbide cores in our piston-cylinder pressure vessels were destroyed to conduct the experiments, representing the most expensive and time-consuming aspect of this project. Experiments were terminated after ~2–5 days by shutting off the power to the graphite furnace (Fig. 1), which quenched the experiment to below 100 °C in less than 30 s. The capsules were opened with two pairs of pliers by wrenching off the capsule lid. Experimental run products



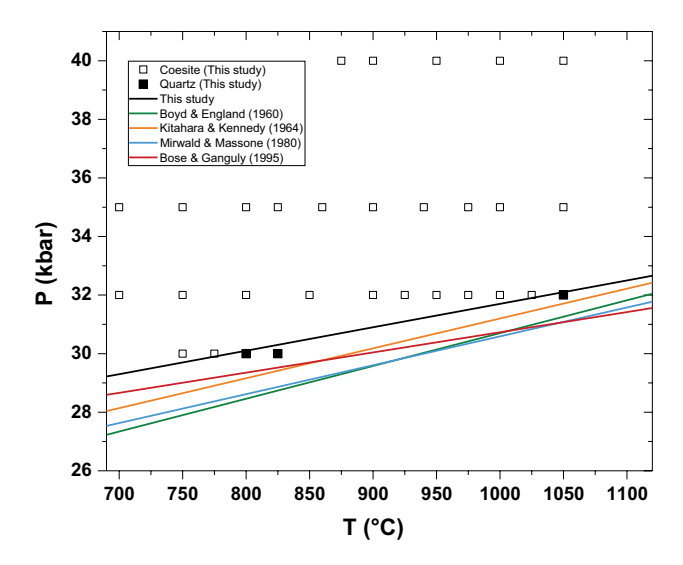


Fig. 2 Experimental P–T conditions and phase relations from this study compared to several previously reported coesite-quartz phase equilibria (Boyd and England 1960b; Kitahara and Kennedy 1964; Mirwald and Massonne 1980; Bose and Ganguly 1995). The open black squares designate experimental P–T conditions that produced coesite; the solid black squares designate experimental P–T conditions that produced quartz

were washed out of capsules with alcohol or water. Coesite crystals were hand-picked (selected for size and lack of visible inclusions), mounted in epoxy, and polished in preparation for subsequent analyses.

Electron probe microanalysis (EPMA) and cathodoluminescence (CL) imaging

The Cameca SXFive electron microprobe at Syracuse University and the Cameca SX100 electron microprobe at Rensselaer Polytechnic Institute were used for trace element measurements of titanium in coesite. Both instruments have cathodoluminescence imaging capabilities that were used to document Ti distribution in silica minerals; CL imaging was performed using 10–20 nA beam currents. All other imaging and quantitative measurements were performed with 15 kV accelerating voltage. Qualitative identification of rutile and zircon inclusions was performed using the Bruker Quantax EDS attached to the SXFive electron microprobe. For quantitative measurements, the five wavelength dispersive spectrometers were tuned, and elements were standardized using silicate and oxide mineral standards (Astimex MINM25-53 quartz and rutile, http://astimex.com/com/ catalog/min.html) by adjusting the beam current to attain ~ 12,000 counts per second for analyte X-rays on gas-flow proportional counters. Trace element measurements of Ti in coesite were performed using a 200-nA beam current and a 'focused' beam (< 1 μm diameter). Titanium Kα X-rays were diffracted with large PET diffraction crystals (22×60 mm)

Table 1 Comparison of SIMS and EPMA analyses

	TiiC-38 SIMS	TiiC-38 EPMA
Average (ppm Ti)	9.8	10
Standard error (1σ)	0.9	0.6
Number of measurements	5	90

and simultaneously counted on four spectrometers (200 s on peak, 100 s on low and high backgrounds), which yielded an average theoretical detection limit of 5 ppm (by weight) for individual measurements. Silicon Kβ X-rays were counted to confirm analyzed materials were silica. To avoid secondary fluorescence effects, care was taken to avoid Ti measurements within ~50 μm of rutile crystals. The accuracy of EPMA measurements was evaluated by analyzing quartz reference materials including synthetic quartz reference materials from Thomas et al. (2010) containing several different titanium concentrations measured independently and/ or by analyzing Herkimer quartz as a Ti-in-quartz blank. One experiment (TiiC-38) was additionally analyzed by Secondary Ionization Mass Spectrometry (SIMS) at Woods Hole Oceanographic Institution. Data from both methods are given in Table 1. Our EPMA routine produced an average Ti concentration of 10 ppm, less than 1 ppm difference from SIMS analyses average Ti concentration of 9.8 ppm. This agreement in measured Ti concentration between analysis methods lends confidence to the validity of our trace element EPMA measurements.

Raman spectroscopy

Raman spectra of coesite, quartz, rutile, and zircon were measured with a Renishaw inVia Raman microprobe in the Department of Chemistry at Syracuse University. Incident 532 nm laser light was focused onto crystals using a 100× objective (NA = 0.9). Spectra were acquired for 20–30 s. Raman shifted light was backscattered (180° geometry) and statically dispersed with 1800 groove/mm gratings onto a charged-couple device. The Renishaw spectrometer has ~0.5 cm⁻¹ spectral resolution (dependent on wavelength of shifted light) and precision of standard measurements is typically <0.1 cm⁻¹. The spectrometer was calibrated against numerous Ne lines, and spectral accuracy and linearity were checked throughout each analytical session by measuring the Rayleigh scattered laser light and the 520.5 cm⁻¹ band of a silicon standard.

X-ray absorption spectroscopy

Titanium K-edge X-ray absorption near-edge structure (XANES) spectra were measured on beamline 13-ID-E at



the Advanced Photon Source (APS) at the U.S. Department of Energy's Argonne National Laboratory to characterize the coordination environment of titanium ions in experimental coesite crystals. With the goal of maximizing count rate, we measured coesite crystals from several of the higher temperature experiments from each isobar (i.e. higher Ti concentration). The edge position for Ti $K\alpha$ was measured on Ti foil at ~4964.5 eV; this is about 1.5 eV lower than the previously accepted and widely used value of 4966 eV. The Athena software program (Ravel and Newville 2005) was used to process and normalize all XANES data. Normalization of XANES spectra permits direct comparison of spectral features of different specimens, independent of Ti concentration and instrumentation settings. The energy of the absorption edge (E_0) was designated by choosing the maximum peak of the first derivative of the spectrum in the edge region ($\sim 4980 \pm 10 \text{ eV}$). The pre-edge and post-edge energy regions were selected to attain a linear fit to each energy region.

Results and discussion

All experiments were conducted in the SiO₂-TiO₂-ZrSiO₄ field of the TiO₂-ZrO₂-SiO₂ system (see Fig. 1 of Thomas et al. 2010) with a stable equilibrium mineral assemblage composed of a silica polymorph, rutile, and zircon, which buffered SiO₂, TiO₂, and ZrSiO₄ activities at their maximum possible values. Experimental conditions listed in Table 2 are shown on Fig. 2 relative to the coesite-quartz phase boundary. Abundant milky-white aqueous fluid was present upon opening experimental capsules; experiments run at higher P-T conditions with less initial water remained visibly wet and exhibited typical crystal growth. Hundreds of coesite, rutile, and zircon crystals grew in each experiment. Coesite crystals ranged in size from $\sim 10 \mu m$ to $\sim 1 mm$; larger crystals generally formed in the higher temperature experiments. Crystals have anhedral to euhedral shapes; many crystals clearly display the monoclinic symmetry of coesite (Fig. 3a). Rutile and zircon crystals are typically less

Table 2 List of experimental run conditions and Ti concentrations

Run #	T (°C)	P (kbar)	Ti (ppm) ^a	$\ln X_{ m TiO_2}^{ m coesitea}$	Time (h)	Number of measure-ments
TiiC-38	700	32	10 (1)	-11.41 (0.05)	72	90
TiiC-55	750	32	28 (1)	-10.35 (0.05)	72	89
TiiC-66	800	32	30 (1)	-10.25 (0.02)	72	208
TiiC-62	850	32	39 (1)	-9.93 (0.02)	72	211
TiiC-48	900	32	61 (2)	-9.48 (0.02)	70	121
TiiC-21	925	32	90 (3)	-9.09(0.03)	120	30
TiiC-25	950	32	103 (2)	-8.99 (0.03)	120	116
TiiC-26	975	32	121 (4)	-8.79(0.03)	120	37
TiiC-61	1000	32	137 (2)	-8.67 (0.01)	72	87
TiiC-64	1025	32	182 (1)	-8.39(0.01)	72	138
TiiC-11	700	35	6 (<1)	-11.76 (0.07)	120	43
TiiC-58	750	35	10 (<1)	-11.37 (0.05)	72	86
TiiC-18	800	35	16 (1)	-10.82 (0.05)	120	13
TiiC-10	825	35	15 (1)	-10.90 (0.03)	120	86
TiiC-6	860	35	21 (<1)	-10.54 (0.02)	120	13
TiiC-4	900	35	35 (1)	-10.03 (0.03)	120	17
TiiC-3	940	35	48 (1)	-9.72 (0.02)	120	34
TiiC-7	975	35	82 (2)	-9.18 (0.02)	142	11
TiiC-53	1000	35	68 (1)	-9.37 (0.01)	72	138
TiiC-68	1050	35	132 (1)	-8.71 (0.01)	72	121
TiiC-17	875	40	19 (1)	-10.62 (0.03)	120	31
TiiC-14	900	40	25 (1)	-10.38 (0.03)	47	14
TiiC-15	900	40	21 (1)	-10.52 (0.04)	120	16
TiiC-16	950	40	41 (1)	-9.88 (0.02)	96	34
TiiC-70	1000	40	55 (1)	-9.58 (0.01)	72	124
TiiC-69	1050	40	93 (1)	-9.06(0.01)	72	118

^aValues in parentheses are one standard error from the mean. Each Ti concentration and $\ln X_{\text{TiO}_2}^{\text{coesite}}$ value is the data set average. Decimal places included are for fitting purposes



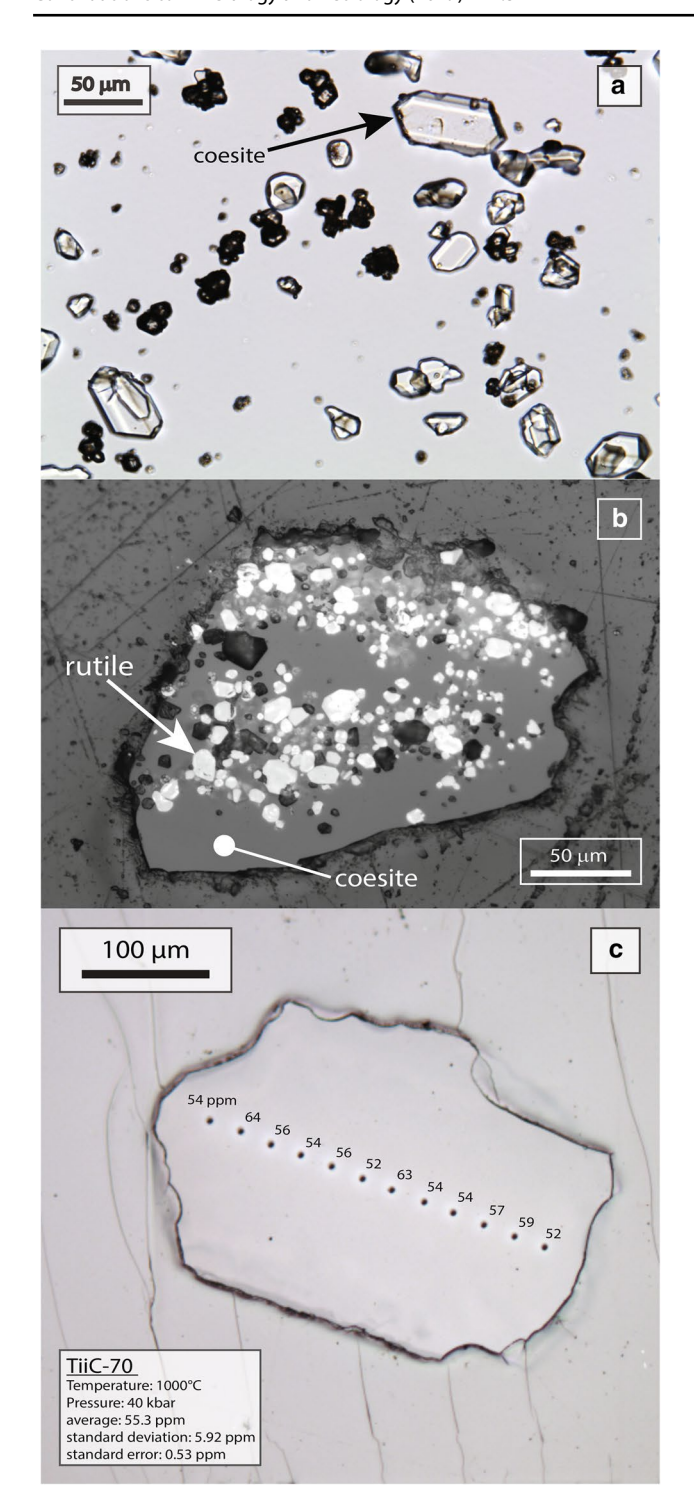


Fig. 3 Mixed reflected and transmitted light photomicrographs of experimental run products. a Loose run products; external forms of some coesite crystals clearly show monoclinic symmetry. b Single coesite crystal mounted in epoxy with inclusions of (bright) rutile and negative crystal forms (dark). c Single coesite crystal mounted in epoxy overlain with titanium concentrations measured by electron microprobe

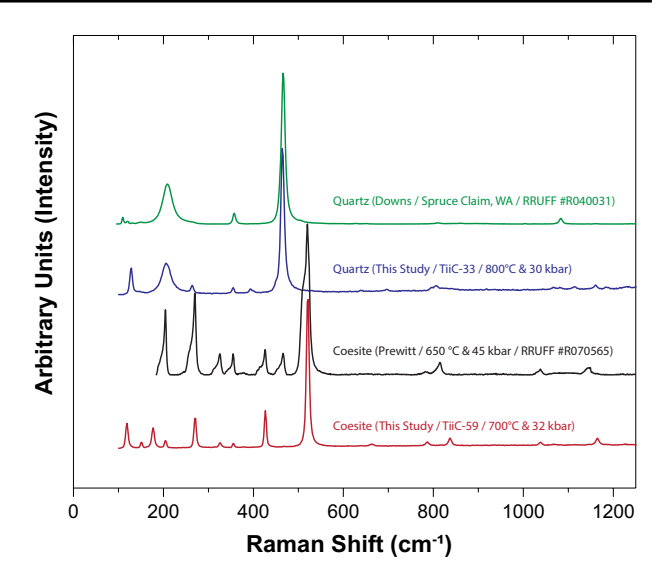


Fig. 4 Raman spectra of synthesized coesite and quartz crystals compared to spectra from the RRUFF database of Raman spectra (Lafuente et al. 2015). The strong peaks of each spectrum are the products of symmetric Si-O-Si stretching-bending vibrations within the silicate ring structures of the mineral (Kingma and Hemley 1994). Coesite Raman band frequencies are significantly different than quartz Raman bands. Additionally, Raman spectra from our study do not show any evidence of quartz crystallites (in the form of Raman Shift peak at ~465 cm⁻¹) sometimes observed in natural coesite (Sharma et al. 1981; Boyer et al. 1985)

than 30 µm, are anhedral to euhedral, and commonly occur as inclusions in coesite (Fig. 3b) demonstrating co-crystallization of the three minerals; the rutile had a characteristic honey-brown color and zircons were colorless.

Cathodoluminescence was used to image coesite crystals prior to quantitative Ti-in-coesite EPMA measurements. Average Ti concentrations in coesite range from ~6 to ~182 ppm (Table 2; Fig. 5). Coesite crystals from each experiment had uniform CL brightness as well as consistent Ti concentrations (Fig. 3c) within single crystals and amongst individual coesite crystals regardless of size and shape.

Raman spectroscopy and the coesite-quartz phase boundary

There is notable variation among previously reported locations of the coesite-quartz phase boundary in P-T space (Mao et al. 2001). At 1000 °C, for example, selected previous studies locate the phase transition at pressures ranging from ~29 to ~31 kbar (Fig. 2). The silica mineral crystallized in our experiments was unambiguously identified as either coesite or quartz using Raman spectroscopy



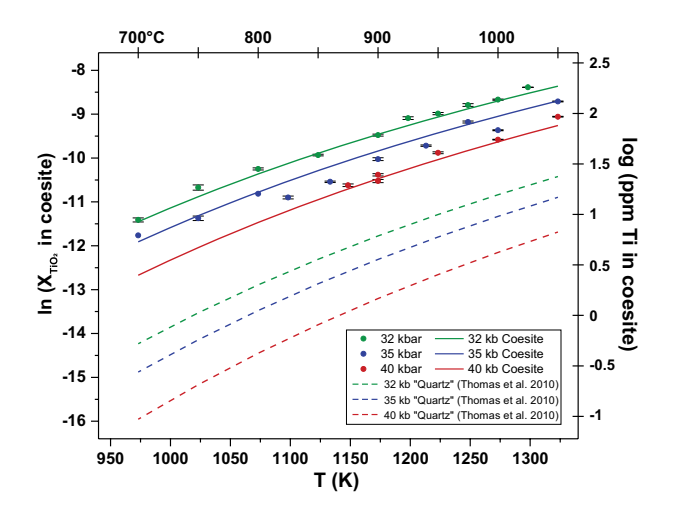


Fig. 5 Ti concentrations of experimentally grown coesite plotted in $\ln X_{\mathrm{TiO}_2}$ vs T (K) space. Error bars are one standard error from the mean and are mostly smaller than the data point symbol. The solid contour lines are least-squares fits to data at each experimental pressure using the empirical fit parameters Eq. (5) obtained from fitting all experimental data to Eq. (4). The dashed lines are the calculated 32, 35, and 40 kbar contour lines using the Ti-in-quartz fit parameters from Thomas et al. (2010)

(Fig. 4), defining P-T points on either side of the coesite-quartz phase boundary. We did not explicitly explore a sufficient temperature range to determine the exact position of the coesite-quartz phase boundary in P-T space; however, we offer an approximate phase boundary and have compared our results to previous studies (Fig. 2). A linear fit to the midpoint between the 775 °C (coesite) and 800 °C (quartz) experiments at 30 kbar and the midpoint between the 1025 °C (coesite) and 1050 °C (quartz) experiments at 32 kbar gives an approximate phase boundary $[P \text{ (kbar)} = 0.0080 \times T \text{ (K)} + 23.7]$ with a slope and position in close agreement with several other reported coesite-quartz phase boundaries (Boyd and England 1960b; Kitahara and Kennedy 1964; Mirwald and Massonne 1980; Bose and Ganguly 1995).

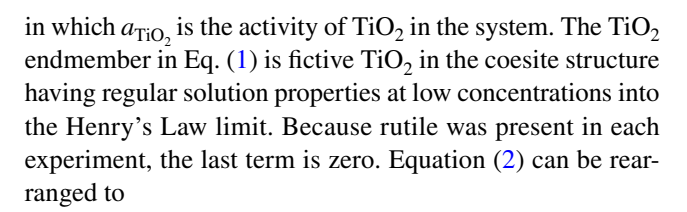
Thermodynamic analysis

When coesite co-crystallizes with rutile, Ti solubility in coesite is governed by the following equilibrium:

$$TiO_2^{coesite} \stackrel{P,T}{\longleftrightarrow} TiO_2^{rutile},\tag{1}$$

where the Ti concentration in coesite varies with P and T. At equilibrium,

$$\Delta \bar{G}^{\circ} = \Delta \bar{H}^{\circ} - T \Delta \bar{S}^{\circ} + P \Delta \bar{V}^{\circ} + RT \ln X_{\mathrm{TiO}_{2}}^{\mathrm{coesite}} - RT \ln a_{\mathrm{TiO}_{2}} = 0, \tag{2}$$



$$\ln X_{\rm TiO_2}^{\rm coesite} = \frac{-\Delta \bar{H}^\circ + T \Delta \bar{S}^\circ - P \Delta \bar{V}^\circ + RT \ln a_{\rm TiO_2}}{RT} \tag{3}$$

and can be fit to the P-T dependent concentrations of Ti in coesite shown in Fig. 5. The temperature dependence of $\ln X_{\rm TiO_2}^{\rm coesite}$ is a function of $\Delta \bar{H}^{\circ}$, and $\Delta \bar{S}^{\circ}$ controls isopleth slopes in P-T space. The experimental data can be simultaneously fit to Eq. (3) using a least-squares approach to characterize the enthalpy, entropy, and volumetric terms related to substituting the significantly different sized Ti⁴⁺ ion for Si⁴⁺.

In the equilibrium defined by Eq. (1), substitution of Ti⁴⁺ for Si⁴⁺ is implicit but the crystallographic site in which Ti resides in the coesite structure and the valence state of Ti ions are not specified. It is conceivable that Ti⁴⁺ ions reside exclusively on tetrahedral sites, but other more complicated incorporation mechanisms are possible. Titanium incorporation could involve a vacancy mechanism with Ti ions dissolved into interstitial sites, Ti ions may occur as Ti³⁺ requiring coupled substitution of a monovalent ion (e.g. H⁺), or other more complicated incorporation mechanisms may occur. Each solubility mechanism would require a unique set of thermodynamic variables to describe the *P-T* dependency of Ti-in-coesite solubility, so there is clear need to obtain information on Ti siting and valence; Ti K-edge XANES measurements can provide this information.

X-ray absorption near-edge structure measurements to probe the Ti coordination environment

Ti K-edge XANES measurements of experimentally grown coesite crystals were used to directly probe the local geometry of the Ti–O polyhedra and provide information on the valence state of Ti ions in coesite. Variations in Ti–O polyhedral geometries can produce up to nine resolvable absorption features in the 4960–5020 eV region. The Ti pre-K-edge absorption in the ~4965 to ~4970 eV region is the most diagnostic because it undergoes the largest changes in position and normalized height as a function of Ti coordination environment and valence state (Fig. 6a) (Waychunas 1987; Farges et al. 1996a, b, 1997; Farges 1997; Berry et al. 2007; Thomas et al. 2010; Tailby et al. 2011). The pre-edge peak intensity significantly decreases and its position shifts to higher energies with increasing



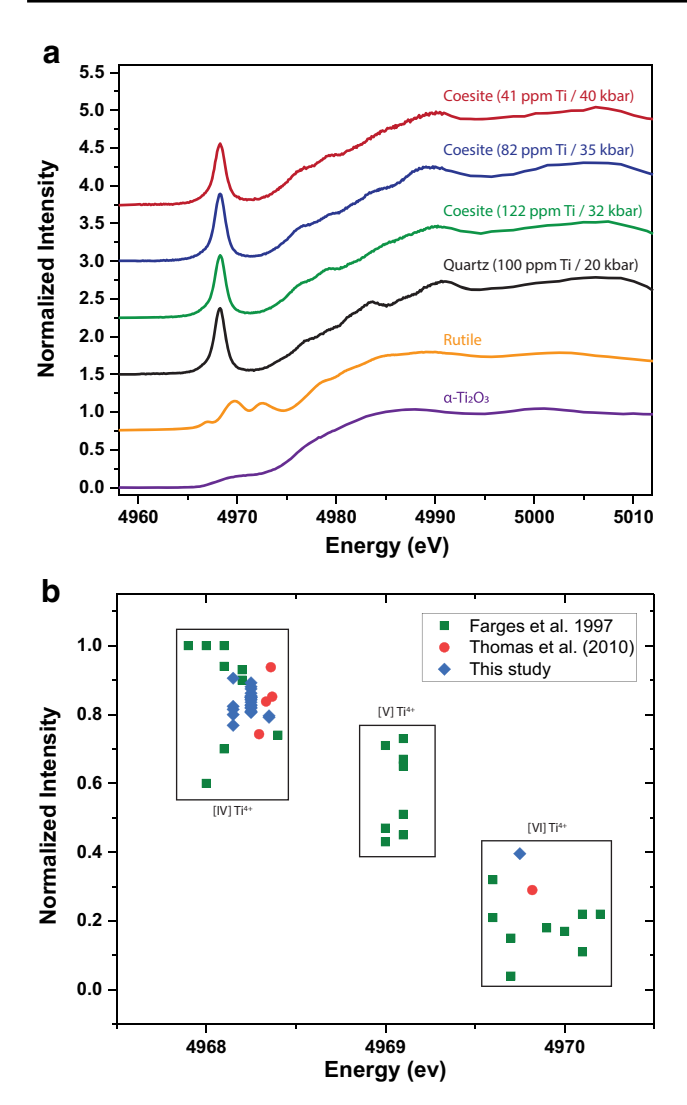


Fig. 6 a Titanium K-edge X-ray absorption near-edge structure (XANES) spectra of synthesized coesite and quartz crystals, a rutile crystal, and α-Ti₂O₃ with corundum structure. The pre-edge peak feature of the coesite and quartz crystals is larger and shifted to lower energies than that of rutile. Raw spectral data were normalized to account for differences in samples and detector settings, and the normalized spectra have been vertically offset for better comparison. b Normalized intensities of pre-edge peak features that occur between the 4968 and 4971 eV photon energy positions. The different boxes group Ti4+ into fourfold [IV], fivefold [V] and sixfold coordination [VI] and include materials from Farges et al. (1997), Thomas et al. (2010), and this study

Ti coordination from four to five to six nearest oxygen neighbors (Fig. 6b). XANES spectra of experimentally grown coesite crystals were compared to high-Ti quartz from Thomas et al. (2010), a rutile reference material, and previously characterized materials that contain Ti in four-, five- and sixfold coordination (Fig. 6b). Coesite XANES spectra were also compared to corundum structure α -Ti₂³⁺O₃ to evaluate the possibility that Ti³⁺ was incorporated into the coesite structure (Fig. 6a).

Titanium K-edge XANES spectral features of our experimental coesite crystals are similar to those of a quartz reference material with 100 ppm Ti (Fig. 6a) that contains Ti⁴⁺ in fourfold coordination (Thomas et al. 2010). XANES spectral features of the coesite are distinct from the rutile. which has Ti⁴⁺ in sixfold coordination and are also distinct from Ti³⁺-containing α-Ti₂O₃ reference materials. Numerous studies provide details on orbital transitions responsible for each of the XANES spectral features observed in the Ti-K-edge region (Bair and Goddard 1980; Waychunas 1987; Farges et al. 1996a, b, 1997; Farges 1997; Berry et al. 2007; Thomas et al. 2010; Tailby et al. 2011; Ackerson et al. 2017; Sutton et al. 2017; Leitzke et al. 2018) so only a brief description is provided here. The octahedral bonding arrangement of Ti⁴⁺ in the rutile structure is responsible for the seven spectral features in Ti K-edge XANES spectra of rutile (Fig. 6a). In general, the pre-edge features with energies less than ~4975 eV are attributed to transitions from Ti 1 s energy levels to bound Ti 3d orbitals. There are several explanations for the three pre-edge spectral features of rutile, but all involve p orbitals of the Ti absorber site mixing with d orbitals of neighboring Ti ions.

Like previous studies of materials with Ti⁴⁺ in fourfold coordination, Ti K-edge XANES spectra of the synthesized coesite crystals have several spectral features that are substantially different from those observed in spectra of rutile (Farges et al. 1996a, b, 1997; Farges 1997; Thomas et al. 2010; Tailby et al. 2011). Compared to rutile, there are subtle differences in the position of the first shoulder and unassigned features that occur on the coesite edge. The most obvious difference between XANES spectra of coesite and rutile occur in the pre-edge region near ~4970 eV (Fig. 6a). Coesite crystals have a pre-edge feature composed of a single peak that has a higher intensity and is shifted to lower energies compared to the multiple pre-edge features observed in rutile spectra. The higher intensity of the pre-edge features observed in spectra of compounds with fourfold Ti⁴⁺ is correlated to the degree of d–p orbital mixing and associated Ti absorber site distortion (Waychunas 1987).

The position of the pre-edge feature of our synthesized coesite crystals is located at a lower energy than the pre-edge feature of rutile (Fig. 6a, b). Coesite crystals have pre-edge peak positions at ~4968.25 eV and the pre-edge feature of our rutile is at 4969.75 eV, energies that agree with previous studies of materials with Ti⁴⁺ in four-, five-, and sixfold coordination, respectively (Fig. 6b). The normalized pre-edge peak intensities of Ti-bearing coesite crystals are considerably higher than the pre-edge feature intensities of rutile, which has Ti⁴⁺ coordinated by six oxygens (Fig. 6a, b). The normalized pre-edge intensities of our coesite crystals (Fig. 6b, multiple blue diamonds in [IV] Ti⁴⁺ box) range from 0.77 to 0.91 (an average of 0.83), which is comparable to the pre-edge intensities previously measured in materials



that contain Ti in fourfold coordination (Farges et al. 1996a, b, 1997; Farges 1997; Thomas et al. 2010; Tailby et al. 2011). The pre-edge intensity feature of rutile measured here is ~0.39 (Fig. 6b, single blue diamond in [VI] Ti⁴⁺ box), which is similar to intensities measured for rutile and other materials in which Ti is in sixfold coordination.

The electronic properties and ionic radii of Ti must strongly influence the solubility of titanium in minerals (Thomas 2016). Titanium generally occurs as Ti⁴⁺ in minerals and melts, but Ti³⁺ is possible in highly reduced systems such as lunar rocks and some meteorites; it is exceptionally rare in terrestrial systems (Anderson et al. 1970; Papike 2005; Borisov 2012; Sutton et al. 2017). It is unlikely that Ti³⁺ was stabilized in our experimental system because the intrinsic oxygen fugacity in our piston-cylinder pressure cells is close to the FeO-Fe₃O₄ oxygen buffer, but it is conceivable that crystal-chemical controls could stabilize Ti³⁺ independent of oxygen fugacity (Doyle et al. 2014). XANES was used to probe for potential Ti³⁺ incorporated into synthesized coesite. Titanium K-edge XANES spectra of Ti³⁺-containing α-Ti₂O₃ are clearly different from those of materials containing Ti⁴⁺ (Waychunas 1987). The nondescript pre-edge and main edge regions in spectra of α -Ti₂³⁺O₃ are characterized by smooth, broad, and poorly resolved features that are shifted by $\sim 1-2$ eV to lower energies than the spectral features of the coesite and rutile crystals (Fig. 6a). XANES spectra of coesite crystals show no evidence for the presence of any Ti³⁺. In all cases XANES spectra indicate that Ti ions are incorporated as Ti⁴⁺ onto the tetrahedral sites substituting directly for Si⁴⁺ in the coesite structure (Fig. 6b).

The effect of pressure and temperature on titanium solubility in coesite: calibration of a Ti-in-coesite solubility model for thermobarometry

XANES measurements confirm that Ti^{4+} substitutes for Si^{4+} on the tetrahedral site in coesite. For this reason, the Ti-incoesite P and T dependencies can be fit to a solubility model that describes Ti-in-coesite solubility at any P and T within the coesite stability field. A model with the form of Eq. (3) was fit to the data from all experiments using a least-squares method (Fig. 5) to the following polybaric expression:

$$RT \ln X_{\mathrm{TiO}_2}^{\mathrm{coesite}} = -a + b \times T \text{ (K)} - c \times P \text{ (kbar)} + RT \ln a_{\mathrm{TiO}_2}^{\mathrm{rutile}}, \tag{4}$$

where the fit parameters a, b, and c are

$$a = 55.068 \pm 4.686$$

 $b = 0.00195 \pm 0.0032$ (5)
 $c = 1.234 \pm 0.113$



Table 3 Least-squares fit parameters obtained by fitting Eq. (4) to Ti-in-coesite solubilities shown on Fig. 5 and listed in Table 2

Parameter	Ti-in-coesite	Zr-in-rutile	Ti-in-quartz
a	55.068 ± 4.686	85.500 ± 0.005	60.952 ± 3.177
b	0.00195 ± 0.0032	0.0291 ± 3	0.00152 ± 0.0039
c	1.234 ± 0.113	0.476 ± 0.039	1.741 ± 0.063
W^{a}	n.d.	0.010	n.d.

^aTomkins et al. (2007) used an interaction parameter (*W*) in their equation to fit Zr-in-rutile solubility due to high Zr concentrations in rutile. Values for Zr-in-rutile are from Tomkins et al. (2007); values for Ti-in-quartz are from Thomas et al. (2010)

n.d. not determined

and $a_{TiO_2}^{\text{rutile}}$ is the activity of TiO_2 in the system referenced to rutile. The a, b, and c terms in Eqs. (4) and (5) are empirical fit parameters that are related to $\Delta \bar{H}^{\circ}$, $\Delta \bar{S}^{\circ}$, and $\Delta \bar{V}^{\circ}$ in Eqs. (2) and (3). Additional fit parameters (e.g. adjustable heat capacity or compressibility terms) were not justified based on uncertainties of our data. We emphasize that the values of fit parameters a, b, and c are substantially different than those obtained for a Ti-in-quartz solubility model (Thomas et al. 2010; Table 3); the estimated 32, 35, and 40 kbar isobars calculated using the Ti-in-quartz solubility model are plotted in Fig. 5. The Ti-in-coesite fit parameters are essential for successful thermobarometric application as it is obvious that the Ti-in-quartz fit parameters do not fit the Ti-in-coesite data. Thus, using the Ti-in-quartz solubility model would underestimate the equilibrium solubility of titanium in coesite.

Using the Ti-in-coesite solubility model as a thermobarometer

The Ti-in-coesite solubility model can be applied as a thermobarometer to coesite-bearing UHP rocks. There are several different ways in which the model can be used to obtain P-T estimates of crystallization. The P-T dependencies of Ti-in-coesite solubility described by Eqs. (4) and (5) can be combined with an independent constraint on either P or T to obtain the pressure and temperature of coesite crystallization. Fortunately, many UHP rocks contain coesite, rutile, and zircon (e.g. Baldwin et al. 2008) which will greatly simplify application of the Ti-in-coesite thermobarometer. Assuming that equilibrium crystallization of coesite, rutile, and zircon will fix SiO₂, TiO₂ and ZrSiO₄ activities at unity, the Ti-in-coesite and Zr-in-rutile solubility models may be simultaneously applied to obtain a crystallization pressure and temperature (Figs. 7, 8; see Tomkins et al. 2007 for details of the Zr-in-rutile thermobarometer). Coesite typically occurs as inclusions contained in other minerals (Figs. 7, 8) and this occurrence as inclusions, such as with

coesite-in-garnet, affords an opportunity to use the crossing point of isopleths calculated from the Ti-in-coesite solubility model and isomekes of elastic thermobarometers (e.g. Angel et al. 2015; Thomas and Spear 2018) to estimate crystallization *P*–*T* conditions, and perhaps timescales of exhumation (e.g. Zhong et al. 2018).

The small size of many natural coesite inclusions and low Ti concentrations will impose some practical limitations and challenges on applying the Ti-in-coesite solubility model as a thermobarometer. Most modern electron microprobes have excellent spatial resolution (~1 µm) and detection limits for Ti of ~5 ppm can be achieved by dedicating multiple spectrometers to the element and employing long acquisition times. Secondary Ion and Laser Ablation Inductively Coupled Plasma Mass Spectrometry instruments can achieve detection limits at the tens of ppb level but spatial resolution is typically $> 10 \mu m$, which may limit the coesite inclusions that can be measured. One must also consider that Ti diffusion may have modified measured Ti concentrations. If analytical challenges can be overcome, it is likely that Ti-incoesite solubility will be widely used for thermobarometric applications to UHP rocks.

As noted previously, Ti-in-coesite solubility can also be combined with an independent constraint on either P or T to obtain the crystallization temperature or pressure. Given a Ti-in-coesite concentration, a known P, and fit parameters listed in Table 3, the temperature can be determined by rearranging Eq. (4) to give

$$T (^{\circ}C) = \frac{a + cP \text{ (kbar)}}{b - R \times \ln X_{\text{TiO}_2}^{\text{coesite}} + R \times \ln a_{\text{TiO}_2}^{\text{coesite}}} - 273.15.$$
 (6)

Given a Ti-in-coesite concentration, a known T, and fit parameters listed in Table 3, the pressure can be determined using

$$P \text{ (kbar)} = \frac{-a + bT \text{ (K)} + RT \times \ln a_{\text{TiO}_2}^{\text{rutile}} - RT \times \ln X_{\text{TiO}_2}^{\text{coesite}}}{c}.$$
(7)

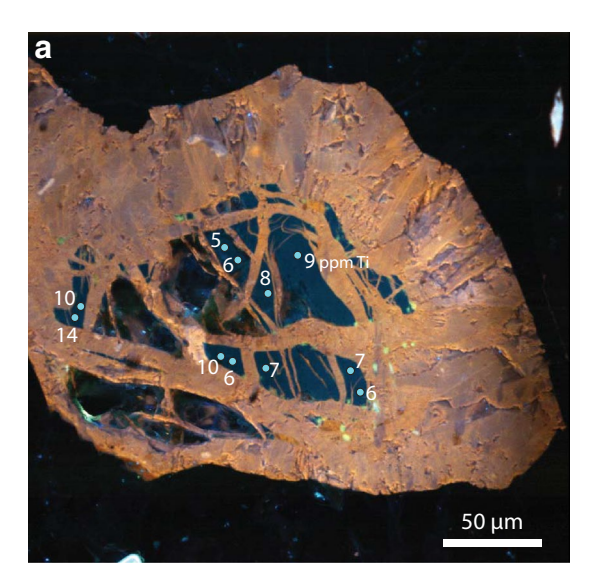
If pressure can be constrained to within ± 1 kbar, the temperature can be estimated to within approximately ± 15 °C. If temperature can be constrained to within ± 25 °C, the pressure can be estimated to within approximately ± 2 kbar.

Applications to coesite-bearing UHP rocks: Dora-Maira, western Alps, Italy

The ultrahigh-pressure section of the Dora-Maira massif, located in the western Alps of Italy, is famously known as one of two localities where coesite inclusions were first discovered in continental rocks (Chopin 1984; Smith 1984). The Dora-Maira UHP rocks are composed of granitic gneisses with intercalated marbles, metabasites, and

whiteschists. Previous research has demonstrated that these rocks have been subducted to depths > 100 km (Chopin et al. 1991; Chopin and Schertl 1999; Rubatto and Hermann 2001; Hermann 2003).

Petrography, CL imaging, and Raman spectroscopic measurements were used to identify coesite contained in a garnet from a Dora-Maira specimen (sample ALP-13E from Jack Cheney, Amherst College). Cathodoluminescence imaging revealed that one SiO₂ inclusion in garnet contained irregular 'relics' of silica with dark CL, which



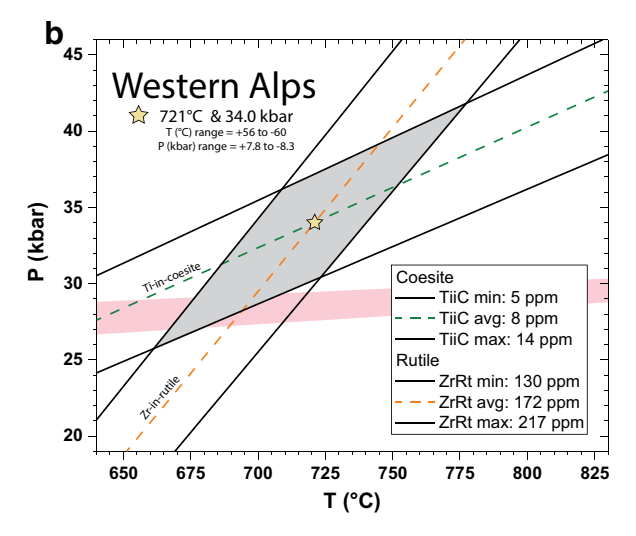


Fig. 7 a CL image of the ALP-13E ${\rm SiO_2}$ inclusion showing the dark blue relics of coesite surrounded by lighter palisade quartz. Concentrations of Ti shown at approximate probe location. **b** Application of the crossing isopleth method to Ti-in-coesite (TiiC) and Zr-in-rutile (ZrRt) data from the western Alps (Dora-Maira) sample ALP-13E (Jack Cheney, Amherst College). The (yellow) star denotes the intersection of the average concentration isopleths at 721 °C and 34.0 kbar. The pink area denotes the approximate quartz–coesite phase boundary region outlined in Fig. 2

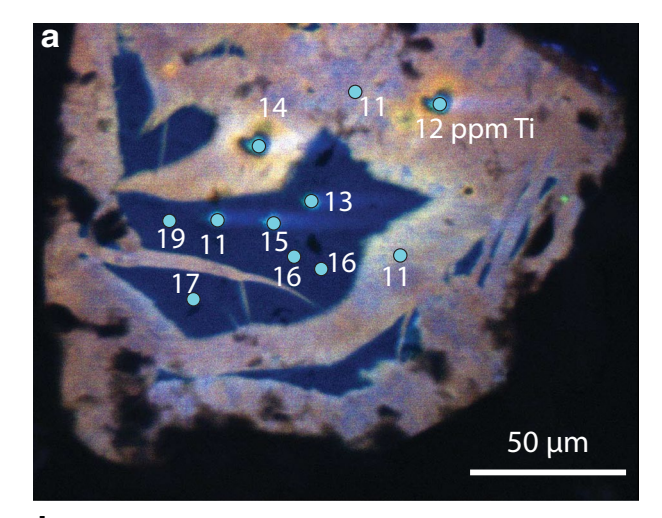


	Western Alps Ti-in-coesite	Western Alps Zr-in-rutile	Papua New Guinea Ti-in-coesite	Papua New Guinea Zr-in- rutile
Average (ppm Ti)	8	172	15	299
Standard error	1	2	1	3
Number of measurements	11	118	9	232

were positively identified as coesite using Raman spectroscopy; these coesite relics were surrounded by bright CL rims of polycrystalline quartz with palisade texture and radial fractures (Fig. 7a). Several coesite relics appeared to have been plucked during polishing. The intact coesite relics that were able to be analyzed contain 8 ± 1 ppm Ti (Table 4). Rutile crystals occur as inclusions in garnets and as crystals dispersed throughout the matrix. The rutile crystals contain 172 ± 2 ppm Zr (Table 4) and there is no apparent difference in Zr concentrations between matrix and inclusion rutile crystals. The Ti-in-coesite and Zr-in-rutile isopleths cross at $721 \pm \sim 58$ °C and $34.0 \pm \sim 8$ kbar (Fig. 7b, yellow star), which is in good agreement with previous peak estimates of 730 ± 30 °C and 43 ± 3 kbar that were based on observed mineral assemblages, whiteschist compositions, experimentally derived petrogenetic grids, and calibrated fluid-absent equilibria (Hermann 2003).

Applications to coesite-bearing UHP rocks: Papua New Guinea

Coesite was discovered in a mafic composition eclogite facies boudin within quartzofeldspathic host gneiss on Tomagabuna Island, part of the D'Entrecasteaux Islands metamorphic core complex in the active Woodlark Rift of eastern Papua New Guinea (Baldwin et al. 2008). The eclogite contains garnet, omphacite, rutile, phengite, quartz (± coesite), and zircon with late stage titanite rimming rutile. Temperature estimates from garnet-pyroxene, Ti-in-zircon thermometry, and Zr-in-rutile thermometry range from ~600 to 760 °C, and pressure estimates based on the jadeite content of omphacite and garnetpyroxene-phengite barometry have given minimum pressures of ~ 18 to 27 kbar (Davies and Warren 1992; Hill and Baldwin 1993; Baldwin et al. 2004, 2008; Monteleone et al. 2007). The presence of a coesite inclusion in omphacite (Fig. 8) indicated that peak metamorphic pressures must have been at least ~28 kbar (Fig. 2) (Baldwin et al. 2008). Like many other occurrences, radial fractures surround the SiO2 inclusion and relict coesite with dark CL are surrounded by bright CL quartz with palisade textures (Fig. 8a). The relict coesite in the inclusion contains an average of 15 ± 1 ppm Ti (Table 4). Rutile crystals occur as inclusions in other minerals and dispersed throughout the matrix. Rutile crystals have 299 ± 3 ppm Zr with a range of 205 to 422 ppm Zr, which is comparable to Zr-in-rutile values reported by Baldwin et al. (2008). These Zr-in-rutile concentrations are also similar to some concentrations measured on



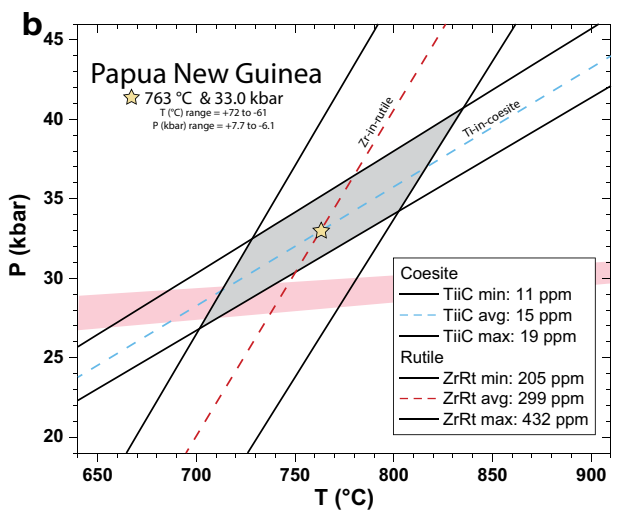


Fig. 8 a CL image of the SiO_2 inclusion (sample 89321C, Baldwin et al. 2008) showing the dark blue relics of coesite surrounded by lighter quartz. Concentrations of Ti shown at approximate probe location. **b** Application of the crossing isopleth method to Ti-in-coesite (TiiC) and Zr-in-rutile (ZrRt) data from PNG sample 89321C. The (yellow) star denotes the intersection of the average concentration isopleths at 763 °C and 33.0 kbar. The pink area denotes the approximate quartz–coesite phase boundary region outlined in Fig. 2



neighboring, non-coesite bearing Papua New Guinea rocks (DesOrmeau et al. 2017, 2018). There are not systematic differences in Zr concentrations between rutile inclusions and matrix crystals. The Ti-in-coesite and Zr-in-rutile isopleths cross at $763\pm\sim65$ °C and $33.0\pm\sim7$ kbar (Fig. 8b, yellow star).

Prior to development of our Ti-in-coesite solubility model, a minimum crystallization pressure was based on the coesite-quartz phase boundary, which is temperature dependent (Fig. 2). Similarly, Zr-in-rutile temperature estimates were based on an assumed crystallization pressure. Recalculation of Baldwin et al.'s (2008) Zr-in-rutile concentrations at 33.0 kbar would give essentially the same temperature as shown in Fig. 8. In summary, previous Zr-in-rutile measurements are in excellent agreement with temperature estimates from combined Ti-in-coesite and Zr-in-rutile thermobarometry (Fig. 8b). As previously noted (Baldwin et al. 2008) and confirmed here, the Ti-in-zircon temperatures are considerably lower than calculated Zr-in-rutile temperatures (Baldwin et al. 2008; DesOrmeau et al. 2017, 2018). The accuracy of Ti-in-zircon temperatures at UHP conditions is uncertain because the pressure effect on Ti solubility in zircon has not been determined, and also because zircon crystallizes over a vast *P*–*T* range and Ti diffusion in zircon is exceptionally slow (Cherniak and Watson 2007).

Titanium diffusion coefficients in coesite are not known. It is notable that the quartz with palisade texture that envelops the coesite inclusions of the Dora-Maira and Papua New Guinea samples has similar Ti concentrations as the coesite inclusions. This occurrence may suggest that Ti concentrations of quartz were not modified by the reconstructive transformation from coesite to quartz. Therefore, it may be possible to apply the Ti-in-coesite solubility model to rocks that contain quartz with palisade texture that was convincingly formed after coesite.

Conclusion

Our experimental results were used to calibrate a Ti-in-coesite solubility model that can be used to estimate *P*–*T* crystallization conditions of coesite-bearing UHP rocks. Titanium K-edge XANES measurements demonstrate that, over the range of pressures investigated here, Ti⁴⁺ substitutes on the fourfold Si⁴⁺ site in coesite. Because a single solubility mechanism operated at all pressures studied, a single set of thermodynamic fit parameters can be used to describe the effect of pressure and temperature on the solubility of Ti in coesite. Combining the Ti-in-coesite and Zr-in-rutile solubility models for thermobarometry to UHP rocks from the Dora-Maira massif gives *P*–*T* estimates that are in excellent agreement with previous investigations. Additionally, thermobarometric applications to the UHP eclogites from Papua New Guinea provide new constraints on peak metamorphic

conditions. Despite the difference in bulk compositions of the coesite-bearing rock units from Dora-Maira (e.g. Chopin et al. 1991) and Papua New Guinea (e.g. Baldwin et al. 2008), it is notable that coesite and rutile from the Dora-Maira and Papua New Guinea specimens have significantly different Ti and Zr concentrations and TitaniC returns *P*–*T* estimates in the UHP field for both.

There are numerous avenues for additional research that would prove useful for applications of Ti-in-coesite solubility as a thermobarometer. As previously noted, six tungsten carbide cores in our piston-cylinder pressure vessels were destroyed conducting these experiments, representing the most expensive and time-consuming aspect of this project. Additional experiments conducted in other devices that can routinely attain higher P-T conditions (e.g. multi-anvil devices) would improve the Ti-in-coesite solubility model. Also, similarities between Ti concentrations in coesite and surrounding quartz with palisade texture that presumably formed from coesite by reconstructive phase transformation during depressurization suggests that enveloping quartz may preserve Ti concentrations that were originally dissolved in the coesite. Unfortunately, Ti diffusion data for coesite do not currently exist. We have abundant quantities of high-Ti coesite crystals with dimensions up to ~1 mm that are available for Ti diffusion in coesite studies. Finally, in our applications to natural samples, we combined the Ti-in-coesite and Zr-in-rutile solubility models. A potential elegant usage would be to combine the Ti-in-coesite solubility model with a coesite-in-garnet elastic model in which *P*–*T* estimates may be determined from the crossing point of Ti-in-coesite isopleths and coesite-in-garnet isomekes (see Wolfe and Spear 2018 for an example combining Zr-in-rutile isopleths and quartz-in-garnet isomekes).

Like other thermobarometric methods, the Ti-in-coesite solubility model is not a simple remedy that can be indiscriminately applied. Combining mineral equilibria requires some assurance that the two minerals co-crystallized in a chemical equilibrium (and the TiO₂ activity is well-constrained) and that subsequent alteration has not affected their compositions. Given these precautions, the Ti-in-coesite solubility model should prove valuable for thermobarometry of UHP rocks. Thermobarometric applications of the Ti-in-coesite solubility model may have implications on lithospheric dynamics studies and could possibly provide additional constraints on subduction and exhumation processes.

Acknowledgements This research was made possible through several grants provided by the National Science Foundation to JBT. Most results were supported by EAR1551343; pilot experiments were performed with funds from EAR1543627. An MRI grant through the NSF Earth Sciences Division (EAR1625835) and support from Syracuse University provided electron microprobe facilities used for much of this research. This research also used resources of the Advanced Photon Source, a U.S. Department of Energy (DOE) Office of Science User



Facility operated for the DOE Office of Science by Argonne National Laboratory under Contract no. DE-AC02-06CH11357. We also acknowledge the support of GeoSoilEnviroCARS (Sector 13), which is supported by the National Science Foundation—Earth Sciences (EAR-1128799), and the Department of Energy, Geosciences (DE-FG02-94ER14466). The XANES measurements at APS would not have been possible without expert support provided by beamline scientists Drs. Lanzirotti and Newville. We thank Tara Kahan at Syracuse University for usage of the Raman spectrometer. Thank you to Jack Cheney at Amherst College for the use of sample ALP-13E. Additional thanks to Kyle Makovsky for comments on an early version of the manuscript. Thank you to Jane Gilotti and Catherine Macris for providing reviews that helped improve the final version of the manuscript.

Appendix

The equation to convert Ti (ppm) to mole fraction TiO_2 in coesite ($X_{TiO_2}^{coesite}$) is:

$$X_{\text{TiO}_2}^{\text{coesite}} = \frac{\frac{\text{Ti (ppm)}}{1E4 \times 0.599 \times 79.87}}{\frac{\text{Ti (ppm)}}{1E4 \times 0.599 \times 79.87} + \left[\left(100 - \frac{\text{Ti (ppm)}}{1E4 \times 0.599 \times 79.87} \right) \times \frac{1}{60.09} \right]}$$

The equation to convert Zr (ppm) to mole fraction ZrO_2 in rutile ($X_{ZrO_2}^{\text{rutile}}$) is:

$$X_{\text{ZrO}_2}^{\text{rutile}} = \frac{\frac{\text{Ti (ppm)}}{1E4 \times 0.74 \times 123.22}}{\frac{\text{Ti (ppm)}}{1E4 \times 0.74 \times 123.22} + \left[\left(100 - \frac{\text{Ti (ppm)}}{1E4 \times 0.74 \times 123.22} \right) \times \frac{1}{79.87} \right]}$$

References

- Ackerson MR, Tailby ND, Watson EB (2017) XAFS spectroscopic study of Ti coordination in garnet. Am Miner 102:173–183. https://doi.org/10.2138/am-2017-5633
- Anderson AT, Crewe AV, Goldsmith JR et al (1970) Petrologic history of moon suggested by petrography, mineralogy, and crystallography. Science 167:587–590. https://doi.org/10.1126/science.167.3918.587
- Angel RJ, Nimis P, Mazzucchelli ML et al (2015) How large are departures from lithostatic pressure? Constraints from host-inclusion elasticity. J Metamorph Geol 33:801–813. https://doi.org/10.1111/jmg.12138
- Bair RA, Goddard WA (1980) Ab initio studies of the X-ray absorption edge in copper complexes. I. Atomic Cu²⁺ and Cu(II)Cl₂. Phys Rev B 22:2767–2776. https://doi.org/10.1103/PhysRevB.22.2767
- Baldwin SL, Monteleone BD, Webb LE et al (2004) Pliocene eclogite exhumation at plate tectonic rates in eastern Papua New Guinea. Nature 431:263–267. https://doi.org/10.1038/nature02846
- Baldwin SL, Webb LE, Monteleone BD (2008) Late Miocene coesite– eclogite exhumed in the Woodlark Rift. Geology 36:735. https:// doi.org/10.1130/G25144A.1
- Berry AJ, Walker AM, Hermann J et al (2007) Titanium substitution mechanisms in forsterite. Chem Geol 242:176–186. https://doi.org/10.1016/j.chemgeo.2007.03.010
- Borisov AA (2012) The Ti⁴⁺/Ti³⁺ ratio of magmatic melts: application to the problem of the reduction of lunar basalts. Petrology 20:391–398. https://doi.org/10.1134/S0869591112040030

- Bose K, Ganguly J (1995) Quartz–coesite transition revisited; reversed experimental determination at 500–1200 °C and retrieved thermochemical properties. Am Miner 80:231–238. https://doi.org/10.2138/am-1995-3-404
- Boyd FR, England JL (1960a) Apparatus for phase-equilibrium measurements at pressures up to 50 kilobars and temperatures up to 1750°C. J Geophys Res 65:741–748. https://doi.org/10.1029/JZ065i002p00741
- Boyd FR, England JL (1960b) The quartz–coesite transition. J Geophys Res 65:749–756. https://doi.org/10.1029/JZ065i002p00749
- Boyer H, Smith DC, Chopin C, Lasnier B (1985) Raman microprobe (RMP) determinations of natural and synthetic coesite. Phys Chem Miner 12:45–48. https://doi.org/10.1007/BF00348746
- Chao ECT, Shoemaker EM, Madsen BM (1960) First natural occurrence of coesite. Science 132:220–222. https://doi.org/10.1126/science.132.3421.220
- Cherniak DJ, Watson EB (2007) Ti diffusion in zircon. Chem Geol 242:470–483. https://doi.org/10.1016/j.chemgeo.2007.05.005
- Chopin C (1984) Coesite and pure pyrope in high-grade blueschists of the Western Alps: a first record and some consequences. Contrib Miner Petrol 86:107–118. https://doi.org/10.1007/BF00381838
- Chopin C, Schertl H-P (1999) The UHP unit in the Dora-Maira Massif, western Alps. Int Geol Rev 41:765–780. https://doi.org/10.1080/00206819909465168
- Chopin C, Henry C, Michard A (1991) Geology and petrology of the coesite-bearing terrain, Dora Maira Massif, Western Alps. Eur J Mineral 3:263–291
- Coes L (1953) A new dense crystalline silica. Science 118:131–132. https://doi.org/10.1126/science.118.3057.131
- Davies HL, Warren RG (1992) Eclogites of the D'Entrecasteaux Islands. Contrib Miner Petrol 112:463–474. https://doi.org/10.1007/BF00310778
- DesOrmeau JW, Gordon SM, Little TA et al (2017) Rapid time scale of Earth's youngest known ultrahigh-pressure metamorphic event, Papua New Guinea. Geology 45:795–798. https://doi.org/10.1130/G39296.1
- DesOrmeau JW, Gordon SM, Little TA et al (2018) Using eclogite retrogression to track the rapid exhumation of the Pliocene Papua New Guinea UHP Terrane. J Petrol. https://doi.org/10.1093/petrology/egy088
- Doyle PM, Schofield PF, Berry AJ et al (2014) Substitution of Ti³⁺ and Ti⁴⁺ in hibonite (CaAl12O19). Am Miner 99:1369–1382. https://doi.org/10.2138/am.2014.4532
- Farges F (1997) Coordination of Ti⁴⁺ in silicate glasses: a high-resolution XANES spectroscopy study at the Ti Kedge. Am Miner 82:36–43
- Farges F, Brown GE, Navrotsky A et al (1996a) Coordination chemistry of Ti(IV) in silicate glasses and melts: II. Glasses at ambient temperature and pressure. Geochim Cosmochim Acta 60:3039–3053. https://doi.org/10.1016/0016-7037(96)00145-7
- Farges F, Brown GE, Rehr JJ (1996b) Coordination chemistry of Ti(IV) in silicate glasses and melts: I. XAFS study of titanium coordination in oxide model compounds. Geochim Cosmochim Acta 60:3023–3038. https://doi.org/10.1016/0016-7037(96)00144-5
- Farges F, Brown GE, Rehr JJ (1997) Ti K-edge XANES studies of Ti coordination and disorder in oxide compounds: comparison between theory and experiment. Phys Rev B 56:1809–1819. https://doi.org/10.1103/PhysRevB.56.1809
- Hazen RM (1999) The diamond makers. Cambridge University Press, New York
- Hermann J (2003) Experimental evidence for diamond-facies metamorphism in the Dora-Maira massif. Lithos 70:163–182. https://doi.org/10.1016/S0024-4937(03)00097-5
- Hill EJ, Baldwin SL (1993) Exhumation of high-pressure metamorphic rocks during crustal extension in the D'Entrecasteaux region,



- Papua New Guinea. J Metamorph Geol 11:261-277. https://doi. org/10.1111/j.1525-1314.1993.tb00146.x
- Kingma KJ, Hemley RJ (1994) Raman spectroscopic study of microcrystalline silica. Am Miner 79:269-273
- Kitahara S, Kennedy GC (1964) The quartz-coesite transition. J Geophys Res 69:5395-5400. https://doi.org/10.1029/JZ069i024p
- Lafuente B, Downs RT, Yang H, Stone N (2015) 1. The power of databases: The RRUFF project. In: Armbruster T, Danisi RM (eds) Highlights in mineralogical crystallography. de Gruyter, Berlin, pp 1-30
- Leitzke FP, Fonseca ROC, Göttlicher J et al (2018) Ti K-edge XANES study on the coordination number and oxidation state of Titanium in pyroxene, olivine, armalcolite, ilmenite, and silicate glass during mare basalt petrogenesis. Contrib Mineral Petrol. https://doi. org/10.1007/s00410-018-1533-7
- Mao H, Sundman B, Wang Z, Saxena S (2001) Volumetric properties and phase relations of silica—thermodynamic assessment. J Alloy Compd 327:253-262. https://doi.org/10.1016/S0925 -8388(01)01465-7
- Mirwald PW, Massonne H-J (1980) The low-high quartz and quartzcoesite transition to 40 kbar between 600° and 1600 °C and some reconnaissance data on the effect of NaAlO2 component on the low quartz-coesite transition. J Geophys Res 85:6983. https://doi. org/10.1029/JB085iB12p06983
- Monteleone BD, Baldwin SL, Webb LE et al (2007) Late Miocene? Pliocene eclogite facies metamorphism, D'Entrecasteaux Islands, SE Papua New Guinea. J Metamorph Geol 25:245-265. https:// doi.org/10.1111/j.1525-1314.2006.00685.x
- Ostapenko GT, Tarashchan AN, Mitsyuk BM (2007) Rutile-quartz geothermobarometer. Geochem Int 45:506-508. https://doi. org/10.1134/S0016702907050084
- Papike JJ (2005) Comparative planetary mineralogy: valence state partitioning of Cr, Fe, Ti, and V among crystallographic sites in olivine, pyroxene, and spinel from planetary basalts. Am Miner 90:277-290. https://doi.org/10.2138/am.2005.1779
- Ravel B, Newville M (2005) ATHENA, ARTEMIS, HEPHAESTUS: data analysis for X-ray absorption spectroscopy using IFEFFIT. J Synchrotron Radiat 12:537-541. https://doi.org/10.1107/S0909 049505012719
- Rubatto D, Hermann J (2001) Exhumation as fast as subduction? Geology 29:3. https://doi.org/10.1130/0091-7613(2001)029%3c000 3:EAFAS%3e2.0.CO;2
- Sharma SK, Mammone JF, Nicol MF (1981) Raman investigation of ring configurations in vitreous silica. Nature 292:140-141. https ://doi.org/10.1038/292140a0
- Smith DC (1984) Coesite in clinopyroxene in the Caledonides and its implications for geodynamics. Nature 310:641-644. https://doi. org/10.1038/310641a0

- Spear FS, Thomas JB, Hallett BW (2014) Overstepping the garnet isograd: a comparison of QuiG barometry and thermodynamic modeling. Contrib Mineral Petrol. https://doi.org/10.1007/s0041 0-014-1059-6
- Sutton SR, Goodrich CA, Wirick S (2017) Titanium, vanadium and chromium valences in silicates of ungrouped achondrite NWA 7325 and ureilite Y-791538 record highly-reduced origins. Geochim Cosmochim Acta 204:313–330. https://doi.org/10.1016/j. gca.2017.01.036
- Tailby ND, Walker AM, Berry AJ et al (2011) Ti site occupancy in zircon. Geochim Cosmochim Acta 75:905-921. https://doi. org/10.1016/j.gca.2010.11.004
- Thomas JB (2016) Titanium. In: White WM (ed) Encyclopedia of geochemistry: a comprehensive reference source on the chemistry of the earth. Springer International Publishing, Cham, pp 1–7
- Thomas JB, Spear FS (2018) Experimental study of quartz inclusions in garnet at pressures up to 3.0 GPa: evaluating validity of the quartz-in-garnet inclusion elastic thermobarometer. Contrib Mineral Petrol. https://doi.org/10.1007/s00410-018-1469-y
- Thomas JB, Watson EB, Spear FS et al (2010) TitaniQ under pressure: the effect of pressure and temperature on the solubility of Ti in quartz. Contrib Mineral Petrol 160:743–759. https://doi. org/10.1007/s00410-010-0505-3
- Thomas JB, Watson EB, Spear FS, Wark DA (2015) TitaniQ recrystallized: experimental confirmation of the original Ti-in-quartz calibrations. Contrib Mineral Petrol. https://doi.org/10.1007/ s00410-015-1120-0
- Tomkins HS, Powell R, Ellis DJ (2007) The pressure dependence of the zirconium-in-rutile thermometer. J Metamorph Geol 25:703–713. https://doi.org/10.1111/j.1525-1314.2007.00724.x
- Wark DA, Watson EB (2006) TitaniQ: a titanium-in-quartz geothermometer. Contrib Mineral Petrol 152:743-754. https://doi. org/10.1007/s00410-006-0132-1
- Watson E, Wark D, Price J, Van Orman J (2002) Mapping the thermal structure of solid-media pressure assemblies. Contrib Miner Petrol 142:640-652. https://doi.org/10.1007/s00410-001-0327-4
- Waychunas GA (1987) Synchrotron radiation XANES spectroscopy of Ti in minerals: effects of Ti bonding distances, Ti valence, and site geometry on absorption edge structure. Am Miner 72:89-101
- Wolfe OM, Spear FS (2018) Determining the amount of overstepping required to nucleate garnet during Barrovian regional metamorphism, Connecticut Valley Synclinorium. J Metamorph Geol 36:79-94. https://doi.org/10.1111/jmg.12284
- Zhong X, Moulas E, Tajčmanová L (2018) Tiny timekeepers witnessing high-rate exhumation processes. Sci Rep. https://doi.org/10.1038/ s41598-018-20291-7

Publisher's Note Springer Nature remains neutral with regard to jurisdictional claims in published maps and institutional affiliations.

